Appendix A: Measurement Resolution and Quality Control

The purpose of this appendix is to describe the techniques we used to determine the resolution of our measurements. We focus on the spectrometer and experiments described in chapter 4, as they were the most sensitive measurements. In these experiments, we detect two particles (one electron and one recoil-ion) for each event with three parameters per particle, for a total of six measured quantities. We explain the method for determining the resolution of each quantity, as well as their respective values. Results from simulations used to model the electrostatic spectrometer are presented, in addition to the results of a direct calibration with a capture measurement. We will conclude with the values of the resolution for each quantity.

A.1 Determination of ΔP_{Rz} and ΔP_{Ry}

In this section we will describe the determination of the recoil momentum resolution in the two dimensions of the recoil detector plane. We used the program SIMION [A.1] to do a simulation of the electrostatic spectrometer. The simulation predicted both the flight times and detector positions of recoil ions produced in the collisions. Shown in figure A.1 is a schematic diagram of the spectrometer (top) along with the SIMION simulation of the equipotential lines and recoil ion trajectories. By adjusting the potentials on the “Grid 1” and “Focus” electrodes, we were able to form an

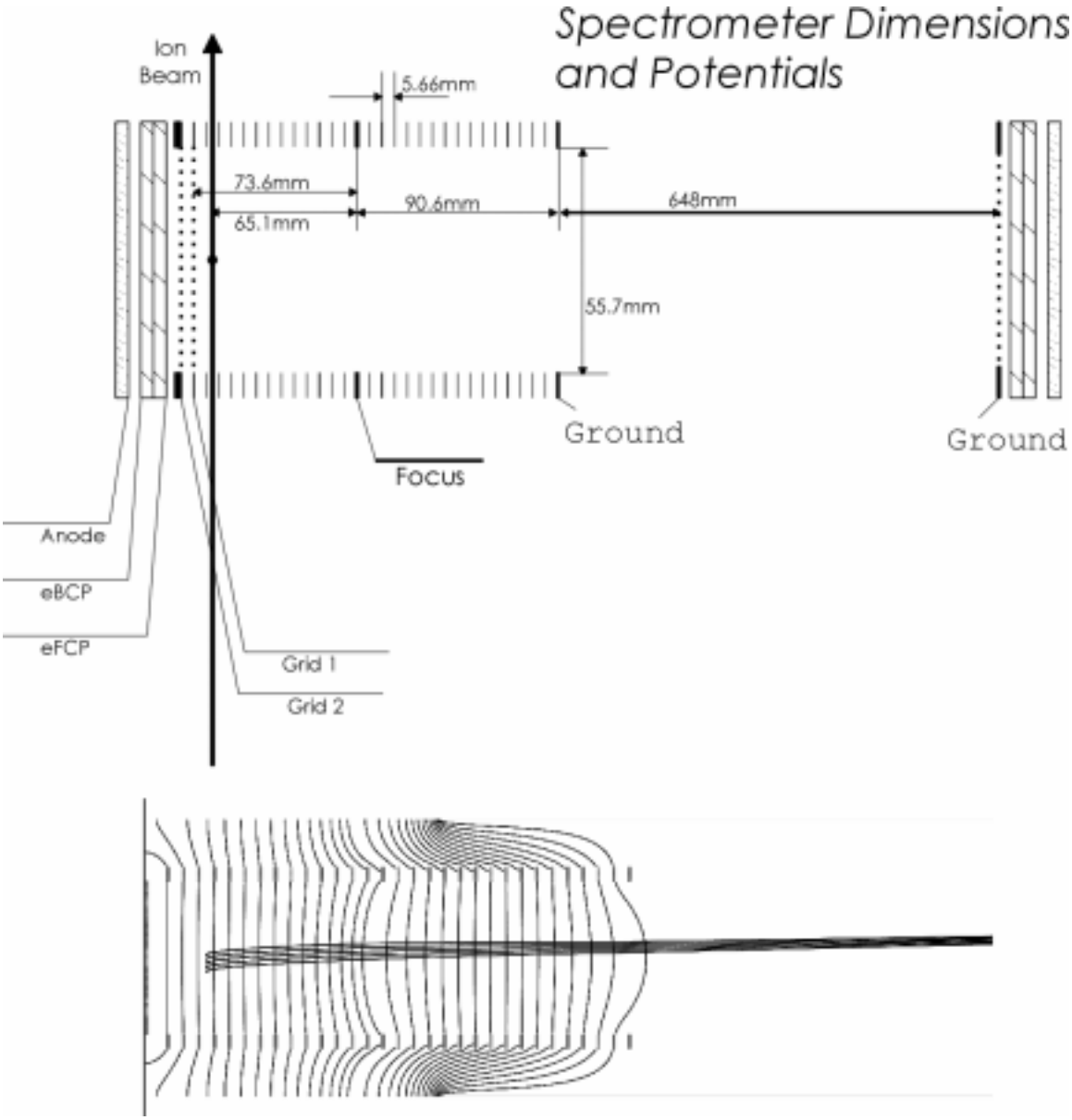

Figure A.1: Schematic of spectrometer dimensions and potentials (top). SIMION generation of equipotential lines (bottom).

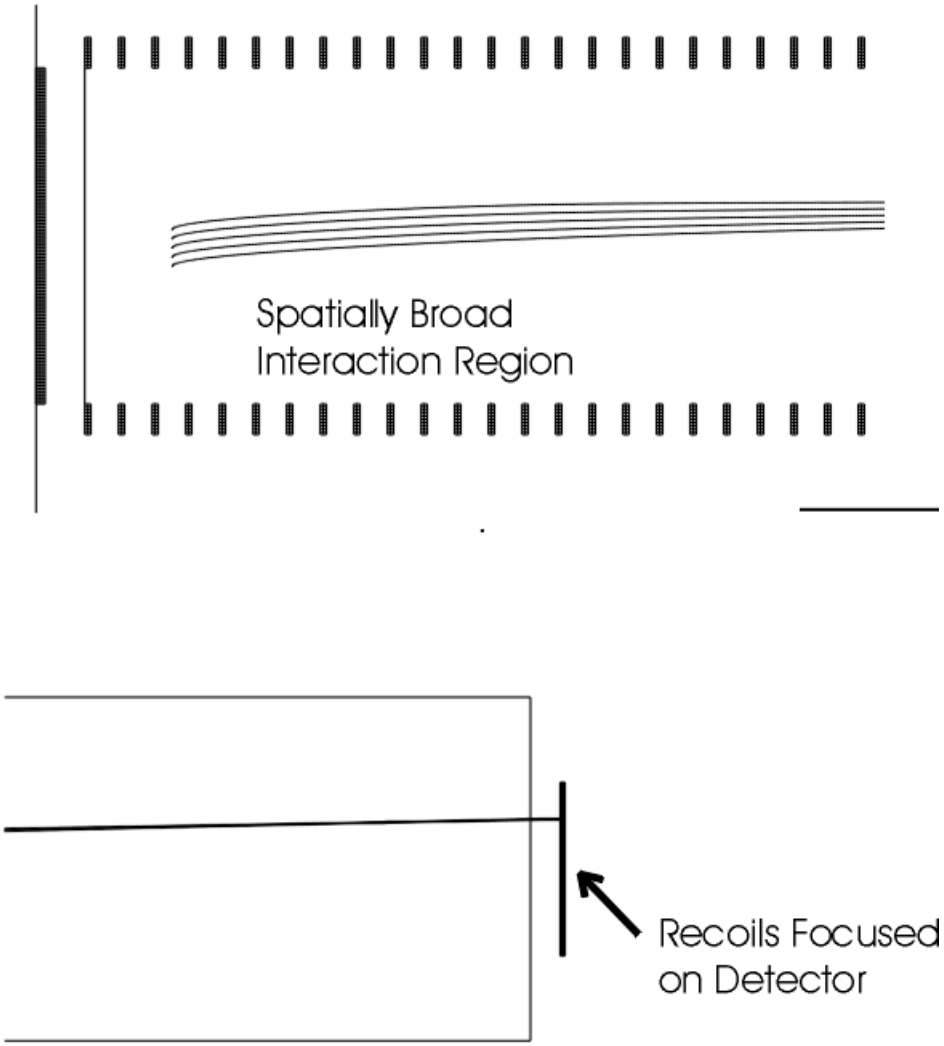

Figure A.2: SIMION images of initial and final spatial distributions of target and detector image.

electrostatic lens that can be seen in the simulation. In figure A.2, we see an example of how the lens allowed us to spatially focus recoil ions formed within the of the target jet (~2 mm) to a point on the recoil detector (<0.5mm). We were thus able to predict the appropriate focus settings prior to taking a measurement.

It was with information from SIMION alone that we performed our early experiments. In this case, although we could do simple tests to assure ourselves the spectrometer was behaving correctly, we had to trust that the calculations predicted the correct focus voltage. In the final set of experiments, however, we did an additional check on the spectrometer calibration. Using the single capture channel of the 1 MeV H^+ + He system, we were able to determine the longitudinal momentum resolution of our spectrometer as well as calibrate the exact position to momentum conversion.

From equation 4.5, we know that the energy transfer in a collision is directly related to the longitudinal momentum transfer to the projectile. In the case of capture, this momentum transfer is quantized, due to the final bound states of the projectile and target. In this calibration, we measure the neutral projectile beam in coincidence with He^+ recoil ions. In addition to the coincidence due to capture, there is a random contribution on the recoil detector corresponding to singly *ionized* recoils. Recoils produced by ionization have a different Q-value than those produced by capture. Therefore, they have a different longitudinal momentum, and can be easily separated on the detector.

Figure A.3 shows the raw recoil detector position (top) and that same position gated on coincidences between the He^+ recoil ions and the neutral projectiles (bottom).

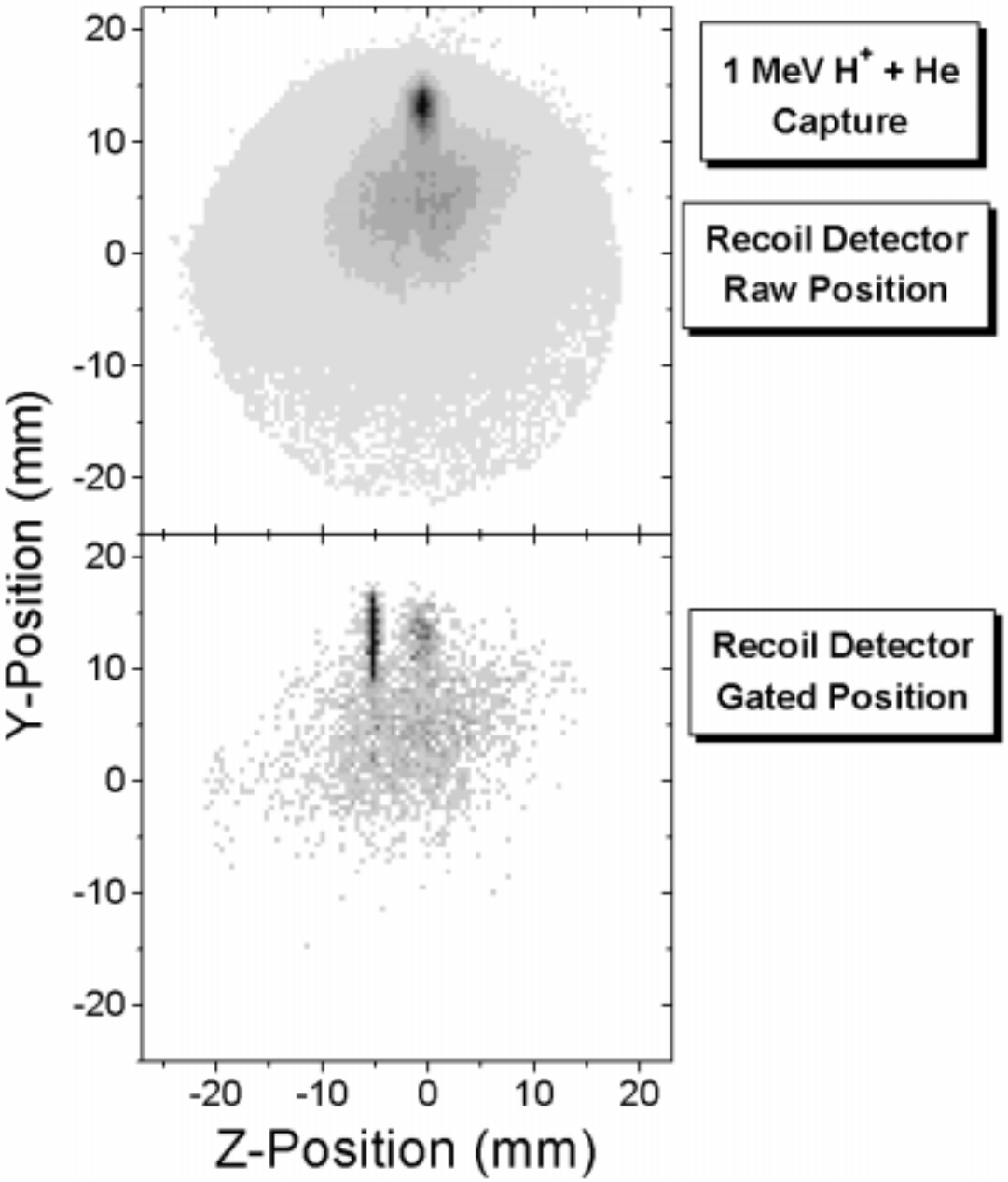

Figure A.3: Recoil detector image for calibration with a capture reaction. The upper plot is the image of the raw detector. The lower plot is the same image gated on the H^0+He^+ coincidence.

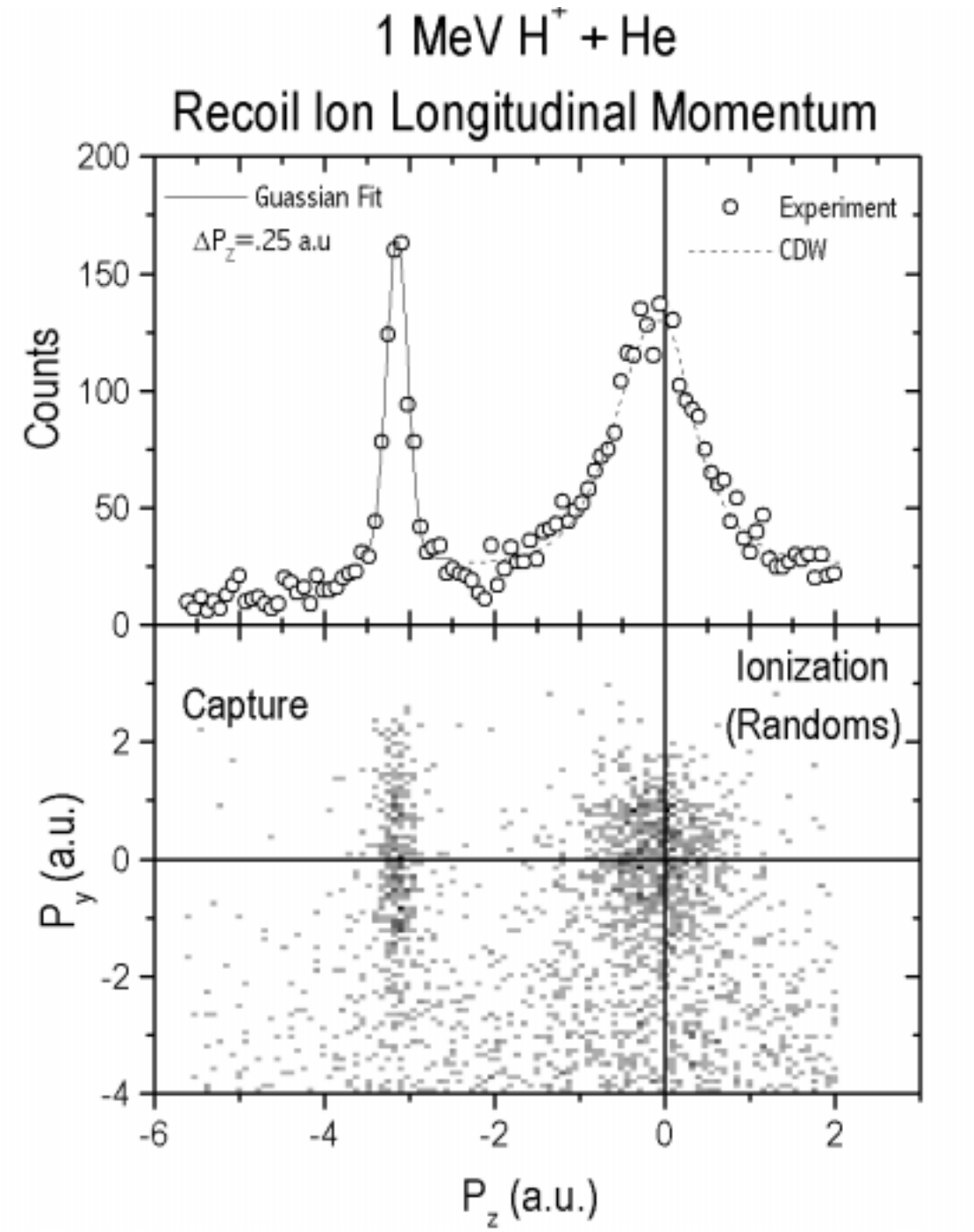

Figure A.4: Enlarged gated detector image (bottom) and projection (top). The capture peak is fit with a guassian, and the ionization peak is matched to CDW theory.

Figure A.4 shows an enlarged view of the gated spectrum (bottom) and a vertical projection (top). There is a clear separation between the true coincidence (capture) and the random coincidence (ionization). From the Q-value equation (4.5) we know the exact separation between the two peaks in momentum ($P_{Rz(capture)}$ = -3.22 a.u.). Therefore, we can accurately determine the momentum to position conversion. In addition, we used this capture line to optimize the focus voltage. The minimum width of the capture peak was 0.25 a.u. The expected momentum width of the gas jet is 0.2 a.u. and makes the dominant contribution this value. The optimum focus voltage for this calibration was in good agreement (< 2%) of the predictions with SIMION.

A.2: Recoil Ion Time Focusing and Determination of ΔP_{Rx}

In the previous sections, we have shown how we have used the lensing characteristics of the spectrometer to spatially focus the collision region onto the recoil detector. However, any width of the projectile beam in the x-direction will also effect the momentum resolution by introducing a width in the time of flight measurement. The spectrometer partially compensates for this, because recoil ions created farther from detector are in the field region longer (allowing for more acceleration). In addition to the effect caused by the beam width, there is an inherent resolution in the time of flight measurement due to electronics.

Figure A.5 shows the results of a calculation based on first principles under the approximation of uniform fields (ignoring the lensing). This gives us an estimate of the

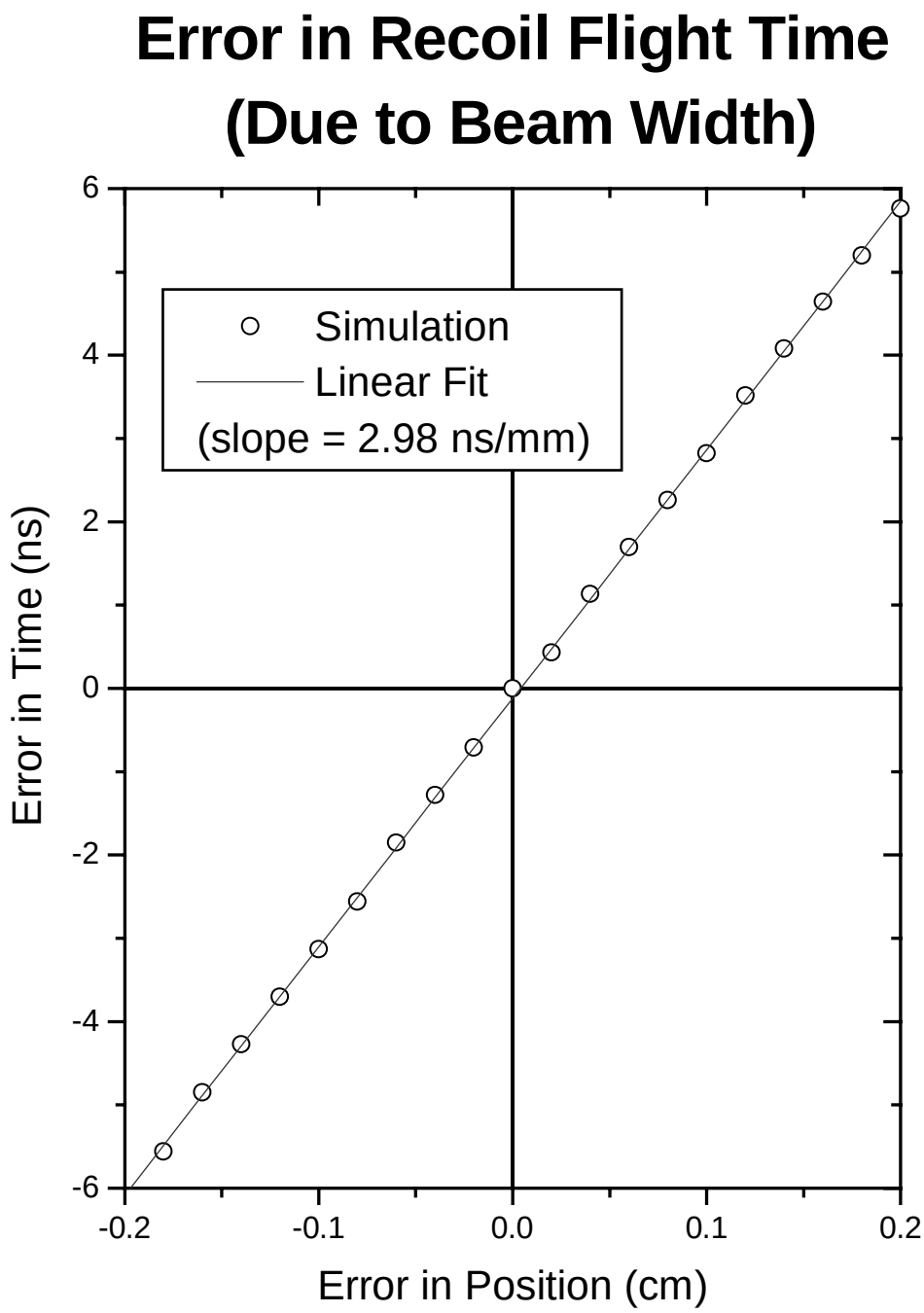

Figure A.5: First principles calculation and fit of the error in the recoil time measurement due to the beam width.

effect of the width of the beam on the error in the time of flight. It is quite significant. A 1 mm wide beam will introduce a 3 nsec width into the time of flight spectrum. The momentum resolution in the direction of the electric field is given by the impulse equation: $\Delta P_{Rx} = Eq\Delta t$. For a typical electric field of 17.4V/cm, this results in a momentum resolution of 0.42 a.u., which is substantial. Combined with the width in time due to electronics, we estimate an upper bound on ΔP_{Rx} to be 0.5 a.u. For the F^{9+} + He system, we used a larger electric field in the spectrometer. This improves Δt due to the width by a factor of $\sqrt{2}$, but the conversion to momentum is worse by a factor of 2. The net result for this case is an upper bound on ΔP_{Rx} of 0.6 a.u.

A.3 Determination of ΔP_{ex}, ΔP_{ey} and ΔP_{ez}

Because the electrons are not spatially focused, the momentum resolution in the z- and y- directions are dominated by the finite width of the gas jet (z-) and beam (y-) at the point of interaction. However, because the momentum calculation is not simply linear with position, but dependent upon the electron flight time, some careful consideration is required. The momentum calculation depends on the flight time by the following relationships:

$$P_y = \frac{m_e\, y}{t} \qquad P_z = \frac{m_e\, z}{t} \qquad \text{A.1}$$

where m_e is the electron mass, t is the time of flight and y,z are the positions on the detector. To first order, the resolution is also time dependent in the following way:

$$\Delta P_y = \frac{m_e\, \Delta y}{t} \qquad \Delta P_z = \frac{m_e\, \Delta z}{t} \qquad \text{A.2}$$

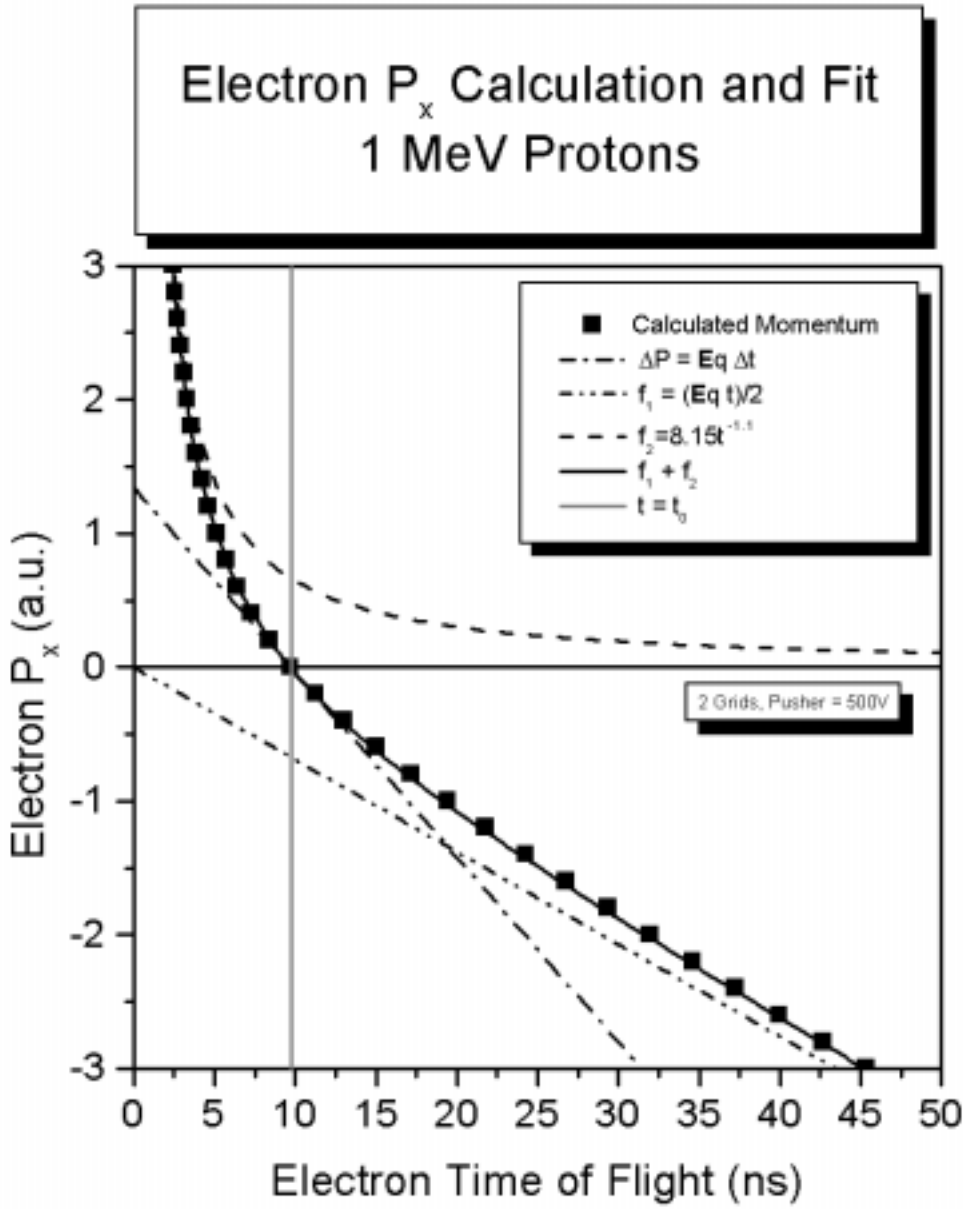

Figure A.6: Calculation and fit of the first principles simulation of $P_{ex}(t)$ for the 1 MeV H^+ +He collisions measurement.

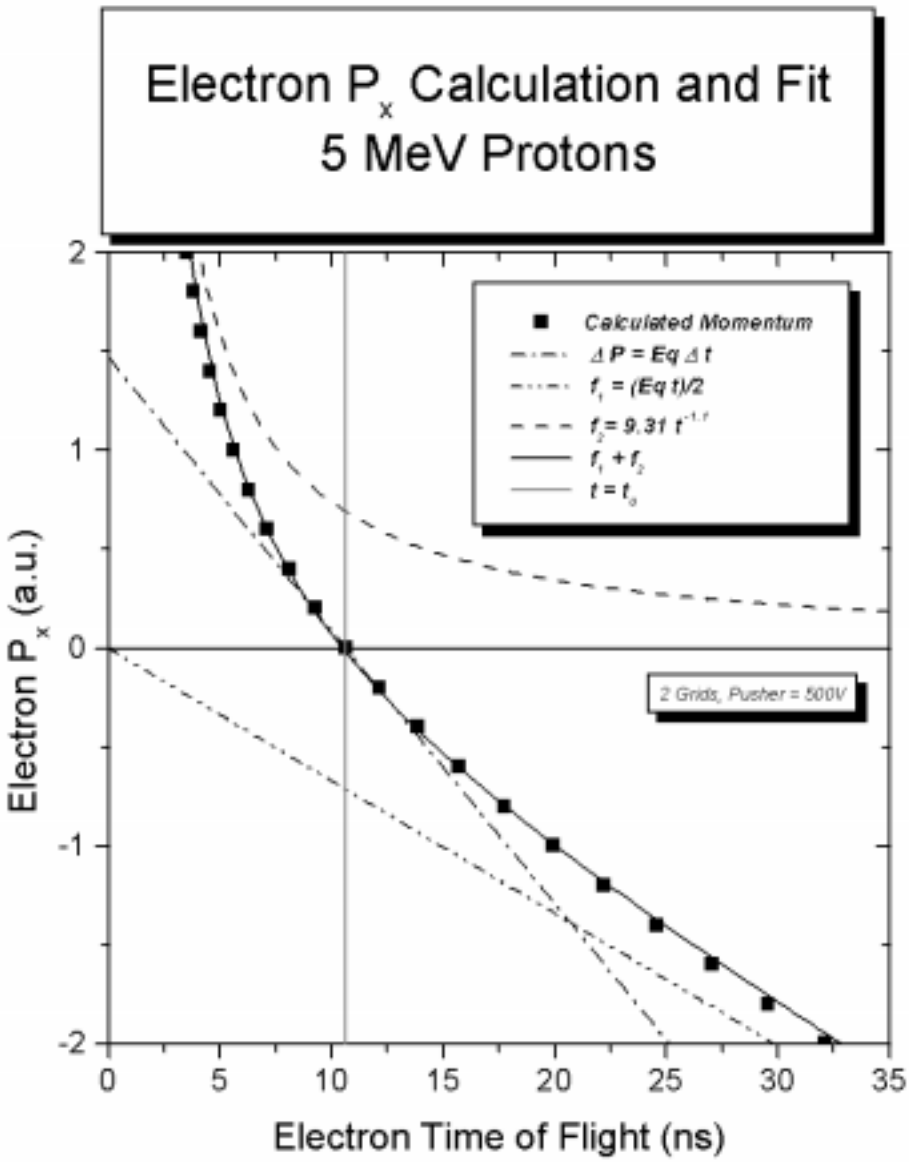

Figure A.7: Calculation and fit of the first principles simulation of $P_{ex}(t)$ for the 5 MeV H^+ +He collisions measurement.

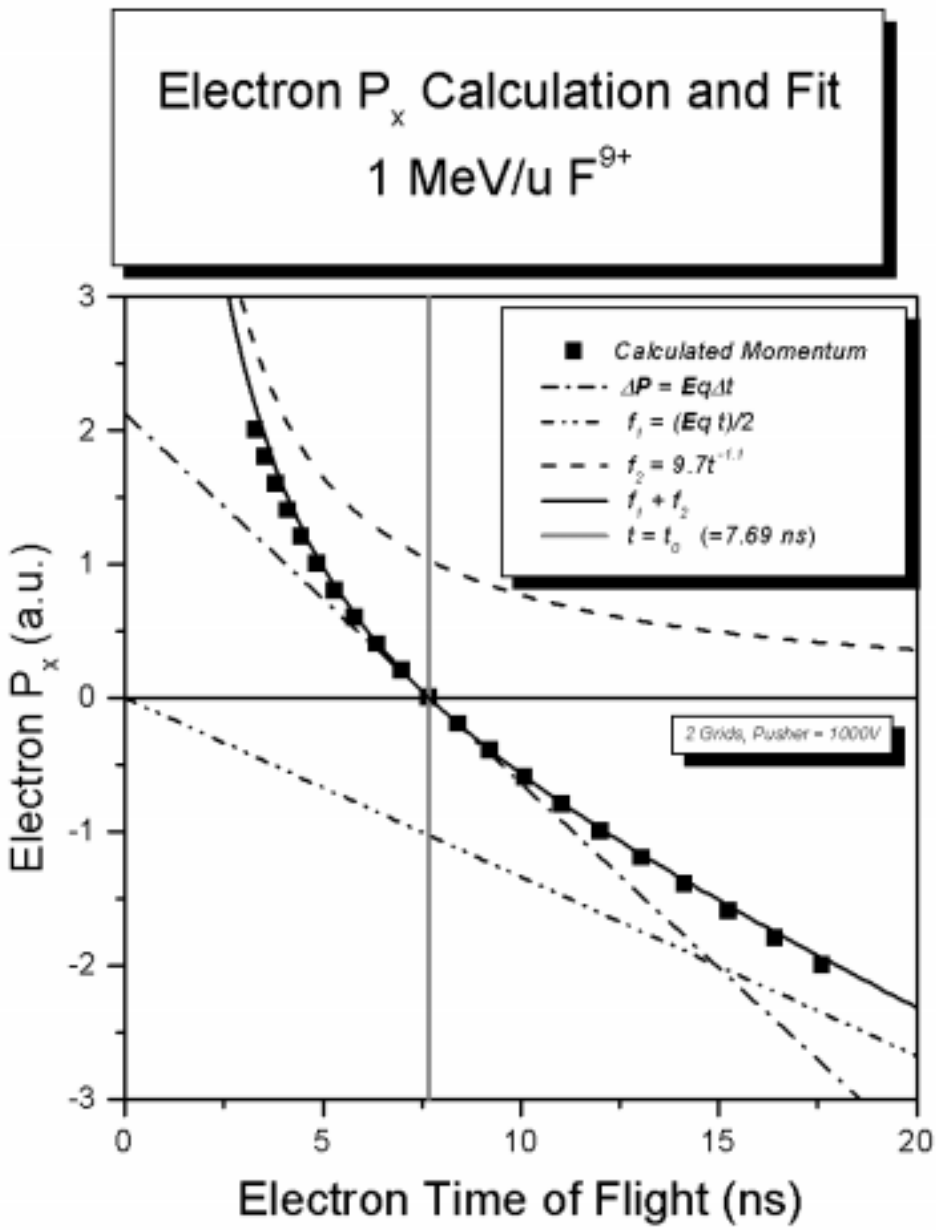

Figure A.8: Calculation and fit of the first principles simulation of $P_{ex}(t)$ for the 1 MeV/u F^{9+} +He collisions measurement.

At the end of the section we will demonstrate this for some examples, using the beam width for Δy (~1 mm), and the jet width for Δz (~2mm).

By design, the focus electrode in the spectrometer is placed far enough away from the collision region to avoid distorting the electron position and flight time. The electron side of the spectrometer has "flat" fields, or no lensing. This allows us to accurately simulate the electron trajectories based upon first principles. For a given electron momentum, it is straightforward to calculate its final position and flight time. Figures A.6, A.7, and A.8 show the calculation for the three field configurations used in our final measurements. The calculated values are then fit with a function so that for a given position and flight time, we can determine the momentum. In the case of the recoil ions this function would be a straight line. However, the electron momentum clearly has a non-linear dependence on P_{ex}. We use the function $P_{ex}(t)$ to determine the momentum from the flight time, and we use its derivative to determine the momentum resolution:

$$\Delta P_{ex} = \frac{dP_{ex}(t)}{dt}\Delta t \,. \qquad \text{A.3}$$

The function $P_{ex}(t)$ was also used to calculate the detector edge in momentum space, as shown in figures 4.13, 4.14 and 4.15.

A.4 Tables of resolution values

Presented below are the calculated values of the momentum resolution for both electric field values, and corresponding to some typical electron flight times.

F^{9+} + He, Pusher = 1000V, E=34.8 V/cm			
Recoil	ΔP_{Rx} (a.u.)	ΔP_{Ry} (a.u.)	ΔP_{Rz} (a.u.)
	0.6	0.25	0.25
electron	ΔP_{ex} (a.u.)	ΔP_{ey} (a.u.)	ΔP_{ez} (a.u.)
P_{ex}=-1 a.u.	0.25	0.03	0.08
P_{ex}= 0 a.u.	0.28	0.05	0.1
P_{ex}= 1 a.u.	0.5	0.09	0.18

1,2,5 MeV H^{+} + He, Pusher = 500V, E=17.4 V/cm			
Recoil	ΔP_{Rx} (a.u.)	ΔP_{Ry} (a.u.)	ΔP_{Rz} (a.u.)
	0.5	0.25	0.25
electron	ΔP_{ex} (a.u.)	ΔP_{ey} (a.u.)	ΔP_{ez} (a.u.)
P_{ex}=-1 a.u.	0.09	0.02	0.04
P_{ex}= 0 a.u.	0.14	0.04	0.08
P_{ex}= 1 a.u.	0.28	0.07	0.14